

Cite this: *J. Mater. Chem. C*, 2023,
11, 8129

Thermal quenching of lanthanide luminescence via charge transfer states in inorganic materials

Pieter Dorenbos 

There are various routes of luminescence quenching such as multi-phonon relaxation from excited states to lower energy states, energy migration to killer sites, and radiation less relaxation to the ground state via the crossing point in a configurational coordinate diagram. In this work, we will consider and review quenching of lanthanide luminescence by means of charge carrier transfer to the valence band or the conduction band of the host compound. We will focus on $4f^n-4f^n$ emission quenching due to thermally activated electron transfer from the $\text{Pr}^{3+} \ ^3\text{P}_0$ level and the $\text{Tb}^{3+} \ ^5\text{D}_4$ level to the conduction band, and due to thermally activated hole transfer from the $\text{Eu}^{3+} \ ^5\text{D}_0$ level to the valence band. In addition, we will consider the quenching of the $4f^{n-1}5d-4f^n$ emission of Eu^{2+} and Ce^{3+} which often (if not always) proceeds by electron transfer to the conduction band. Since all the above quenching routes involve reduction or oxidation of lanthanides, the location of the lanthanide charge transition levels with respect to the host bands is crucial. In other words, we need to know the location of the ground and excited states in the band gap or equivalently the vacuum referred binding energies (VRBE) in the lanthanide states as can be established using the (refined) chemical shift model. A clear correlation between the temperature T_{50} at which luminescence intensity or luminescence decay time has dropped by 50% and thermal quenching activation energies ΔE derived from VRBE schemes will be demonstrated. Since T_{50} typically changes 400–800 K with a 1 eV change in ΔE , and since VRBE energies may contain 0.3–0.5 eV error, it will be clear that the accurate prediction of quenching temperatures from the VRBE data is not yet feasible. Nevertheless, one may derive trends and provide guidelines on how to improve the thermal stability of luminescence.

Received 19th October 2022,
Accepted 1st December 2022

DOI: 10.1039/d2tc04439k

rsc.li/materials-c

Anniversary statement

Ten years ago, the *J. Mater. Chem. C* was a 'new kid on the block' in our field of luminescence phosphors. It has evolved quite rapidly into a high impact factor journal publishing manuscripts related to luminescence materials and their application in devices. We together with collaborating groups have almost yearly published manuscripts in *JMCC* on topics such as thermal quenching in Ce doped garnets, persistent luminescence, carrier dynamics and trapping in phosphors, computational studies on the spectroscopy of lanthanides, and conduction and valence band engineering of phosphor properties. The high impact factor is reflected in the frequency of citations to our work.

1 Introduction and theory

The thermal quenching of luminescence is an important phosphor characteristic for many different applications. For application at room temperature, the onset for thermal quenching should obviously be well above 300 K. Luminescent phosphors in modern day light emitting diode (LED) lighting like Ce^{3+} doped garnet $\text{Y}_3\text{Al}_5\text{O}_{12}$ typically operate at temperatures around 100 C,¹ and phosphors should not start to quench then. High

power white light emitting (WLED) phosphors require thermal stability up to at least 200 C (475 K).^{1,2} The thermal quenching of emission intensity or emission decay time is also used in thermometry.^{3–5} Thermal barrier coating phosphors (TBCs) are used to sense the temperature in turbine engines up to temperatures as high as 1200 K, see, *e.g.*, ref. 6 and 7. Understanding how the quenching temperature depends on the type of the luminescence activator and the type of host compound is then important for research and development, or even for engineering of new phosphor materials towards a specific application. Luminescence intensity can be decreased by various quenching mechanisms as illustrated in Fig. 1 where a luminescence center with a ground state (g.s.) and several

Delft University of Technology, Faculty of Applied Sciences, Department of Radiation Science and Technology, Mekelweg 15, 2629 JB Delft, The Netherlands.
E-mail: p.dorenbos@tudelft.nl; Tel: +31 15 2781336



the highly systematic changes in the level location with the number n of electrons in the $4f^n$ -orbital of the lanthanides which is then combined with the spectroscopic data retrieved from the archival literature. It provides the so-called vacuum referred binding energy (VRBE) diagrams where all divalent and trivalent lanthanide ground and excited state levels are drawn with respect to the VB-top and CB-bottom and also with respect to the vacuum level. This work deals with about 170 different inorganic compounds, and for each compound the available spectroscopic data on the host and on divalent and trivalent lanthanides were gathered and combined to construct their VRBE diagrams. It is not doable to provide the references and analysis for each piece of data used (it would run into many 1000), and the reader has to trust that everything was performed with best scientific effort. Many VRBE schemes have already appeared in the literature where many references to the original data can be found. The reader may also conduct own search in the archival literature to derive, verify or improve the parameters used. The relevant parameters in the VRBE construction will be tabulated for each host and only the reference to information on the thermal quenching data will be provided.

A. Arrhenius equation, the chemical shift model and the VRBE scheme

The thermal quenching of luminescence intensity $I(T)$ is traditionally expressed using the single barrier Arrhenius equation

$$I(T) = \frac{I(0)}{1 + \frac{\Gamma_0}{\Gamma_\nu} \exp\left(\frac{-\Delta E}{k_B T}\right)} \quad (1)$$

where Γ_ν is the radiative decay rate, Γ_0 is the attempt rate for thermal quenching which has similar magnitude as the maximum phonon frequency in compounds, k_B is the Boltzmann constant, and ΔE is the energy barrier for thermal quenching.

A similar equation applies for the lifetime $\tau(T)$ of the excited state

$$\tau(T) = \frac{\tau_\nu}{1 + \frac{\Gamma_0}{\Gamma_\nu} \exp\left(\frac{-\Delta E}{k_B T}\right)} = \frac{I(T)}{I(0)} \tau_\nu \quad (2)$$

where τ_ν is equivalent to $1/\Gamma_\nu$.

Depending on whether defects or dislocations happen to be nearby the activator or not, ΔE may change from activator to activator and therefore become spatial dependent. In cases where quenching proceeds by electron transfer to the CB or hole transfer to the VB, ΔE will also show a temperature dependence because the bandgap of the host compound will be temperature dependent. Due to lattice expansion when the temperature increases the (mobility) bandgap reduces typically by 0.05 eV per 100 K temperature increase. Therefore, the often made assumption of a temperature independent and a single value ΔE fails largely in practice. Furthermore, the radiative decay time usually shows a temperature dependence, *i.e.*, it tends to increase with the temperature increase, see *e.g.* the quenching curves in ref. 11. Considering all the above, a single barrier Arrhenius fit to an experimental quenching curve will

not provide good parameters for the activation energy and frequency factor. Instead of fitting, we will use a fixed value for Γ_0 and estimate the average quenching energy barrier ΔE from the temperature where the luminescence intensity or decay has decreased by 10% (T_{10}) or 50% (T_{50}).

Using eqn (1) and (2), one obtains

$$T_{50} = \frac{11\,600}{\ln(\tau_\nu \Gamma_0)} \Delta E \quad (3)$$

and

$$T_{10} = \frac{11\,600}{\ln 9 + \ln(\tau_\nu \Gamma_0)} \Delta E \quad (4)$$

where Γ_0 depends on the type of compound and ranges from 4×10^{12} Hz for iodide compounds with weakly bonded heavy ions up to 4×10^{13} Hz for strongly bonded borate and phosphate compounds.¹² This corresponds with phonon energies ranging from 130 cm^{-1} to 1300 cm^{-1} . In this work, we adopt the same typical value of $\Gamma_0 = 2 \times 10^{13}$ Hz for each compound. For each lanthanide (A), we adopted a typical decay time τ_ν , as listed in Table 1. The nature of the transitions and their typical emission wavelengths λ are also compiled in Table 1. Those for Tb^{3+} , Pr^{3+} , and Eu^{3+} are almost independent of the type of compound but those for the 5d–4f emissions of Eu^{2+} and Ce^{3+} depend strongly as illustrated in Fig. 2. Since the product $\tau_\nu \Gamma_0$ appears as an argument in the natural logarithm of eqn (3), a factor 4 error in $\tau_\nu \Gamma_0$ will lead to only 5% error in T_{50} . The dependences of T_{50} and T_{10} on ΔE in columns 5 and 6 are obtained using eqn (3) and (4). The ratio, or the slope in K eV^{-1} , increases with a shorter decay time of the luminescence.

B. Chemical shift model with the characteristic VRBE diagram

Fig. 3 shows the vacuum referred binding energy diagram for the lanthanides in YPO_4 as constructed using the (Refined) Chemical Shift model. The model was first introduced in 2012⁸ and refined later in 2019.^{9,10} The diagram shows the location of the divalent and trivalent ground states within the band gap and relative to the vacuum level. The vacuum referred binding energies are equivalent to the $\text{Ln}^{3+/2+}$ and $\text{Ln}^{4+/3+}$ charge transition levels. The most crucial parameter needed to construct a VRBE scheme is the U -value defined as the energy difference between the $\text{Eu}^{3+/2+}$ and $\text{Eu}^{4+/3+}$ CTLs which was determined as 7.09 eV for YPO_4 . The chemical shift model relates the U -value

Table 1 The dependences of T_{50} and T_{10} on the activation energy ΔE calculated for $\Gamma_0 = 2 \times 10^{13}$ Hz and using the typical value for τ_ν in column 4

A	Transition	λ (nm)	τ_ν	$T_{50}/\Delta E$ (K eV ⁻¹)	$T_{10}/\Delta E$ (K eV ⁻¹)
Eu ³⁺	⁵ D ₀ → ⁷ F _{1,2}	≈ 610	2 ms	475	435
Tb ³⁺	⁵ D ₄ → ⁷ F ₅	≈ 545	2 ms	475	435
Pr ³⁺	³ P ₀ → ³ H _{4,5,6}	490, 550, 620	50 μs	560	510
Eu ²⁺	5d → 4f [⁸ S _{7/2}]	380–600	1000 ns	690	610
Ce ³⁺	5d → 4f [² F _{5/2,7/2}]	300–550	40 ns	850	735



was found which agrees well with the prediction from eqn (4) as listed in Table 1.

In this work, we added new information. We selected compounds with a relatively low Eu^{3+} concentration (about 1%). Often, the data for decay time quenching were preferred over those of intensity quenching because the latter tend to be less accurate. The results are shown in Fig. 4 and the data and references are found in Table 2. We also added information on E^{ex} and the U -values from which the data on E_{V} and E_{C} are obtained using the refined chemical shift model. The typical error bars are ± 0.12 eV in the CT-energy and ± 50 K in the T_{10} value. ΔE on the horizontal axis was obtained by

$$\Delta E = E^{\text{CT}} - E(^5\text{D}_0) - 5 \times 10^{-5} T_{10} E^{\text{ex}} \quad (5)$$

where $5 \times 10^{-5} T_{10} E^{\text{ex}}$ is the estimated lowering of the bandgap at a temperature T_{10} where we assumed that the amount of lowering scales with E^{ex} . This is motivated as follows. The VRBE of cation electrons lowers (becomes more negative) when neighboring anions move further away; this is simply a matter of less Coulombic repulsion from the negatively charged anions. The VRBE of anion electrons raises (becomes less negative) when neighboring cations move further away; this is a matter of decreased Coulombic attraction from the positively charged cations. As a result, the cation related CB-bottom moves down and the anion related VB-top moves up causing the bandgap to decrease. For Eu^{2+} , being a cation, we will assume that its VRBE lowers with the same pace as the CB-bottom. Since the VB-top moves upwards, ΔE will decrease with the same amount as the bandgap lowering.

There are few outliers notably ScBO_3 , ScPO_4 and YVO_4 as shown in Fig. 4. Disregarding these, a linear least square fit through the data yields the dashed line with a slope of 421 K eV^{-1} which agrees very good with a predicted value of 435 K eV^{-1} as shown in Table 1. The compound to compound variation in decay time, in maximum phonon frequencies, and

Table 2 Data on T_{10} values for the $\text{Eu}^{3+} ^5\text{D}_0$ emission and the quenching energy barriers ΔE derived from E^{CT} and E^{ex} energies. The parameters used for the VRBE-diagram construction are provided. All energies are in eV

A	U	E^{CT}	E_{V}	E^{ex}	E_{C}	ΔE	T_{10}	Ref.
LaOCl	6.65	4.20	-8.10	6.45	-1.32	1.85	550	19
YOCl	6.65	4.54	-8.44	7.10	-0.94	2.14	630	20
YOBr	6.57	4.32	-8.18	6.50	-1.34	1.93	650	20
LaPO ₄	7.18	4.84	-9.00	8.10	-0.38	2.37	720	7
LuPO ₄	7.08	5.74	-9.85	8.70	-0.55	3.09	1085	7,21
ScPO ₄	7.02	5.95	-10.0	7.40	-2.19	3.42	950	7,22
LaBO ₃	6.93	4.51	-8.54	7.05	-1.10	2.10	650	23,24
ScBO ₃	6.86	5.44	-9.44	7.10	-1.94	3.01	700	24
Ca ₂ Gd ₆ (SiO ₄) ₆ O ₂	6.80	4.59	-8.56	7.00	-1.17	2.20	600	7
X ₂ -Y ₂ SiO ₅ :(Ce1)	6.86	4.80	-8.80	6.82	-1.61	2.32	890	7,25
LaAlO ₃	6.76	3.91	-7.86	6.10	-1.47	1.58	500	26
GdAlO ₃	6.75	4.75	-8.70	7.36	-0.90	2.31	700	4
Y ₃ Al ₅ O ₁₂	6.77	5.23	-9.19	7.10	-1.69	2.69	1020	7
Li ₂ Mg ₂ (WO ₄) ₃	7.15	4.07	-8.21	4.70	-3.34	1.78	465	27
YVO ₄	6.80	4.10	-8.07	4.00	-3.94	1.76	800	7
MgLa ₂ TiO ₆	6.68	3.88	-7.79	4.50	-3.13	1.60	410	28
Gd ₂ Ti ₂ O ₇	6.79	3.94	-7.91	4.15	-3.62	1.68	400	29
Y ₂ Ti ₂ O ₇	6.79	3.85	-7.82	4.25	-3.42	1.56	500	2
Zr _{0.83} Y _{0.17} O _{1.91}	6.70	4.34	-8.26	5.40	-2.63	1.96	740	7,30
La ₂ Zr ₂ O ₇	6.66	4.43	-8.33	6.00	-2.05	2.06	620	5,31
La ₂ Hf ₂ O ₇	6.65	4.40	-8.30	6.00	-2.01	2.03	625	5,31
La ₂ Be ₂ O ₅	6.70	4.11	-8.03	6.28	-1.44	1.78	480	32
Gd ₂ Zr ₂ O ₇	6.65	4.81	-8.71	6.00	-2.42	2.41	725	6
C-Gd ₂ O ₃ :(S ₆)	6.60	4.86	-8.74	5.50	-2.99	2.47	775	33
C-Y ₂ O ₃ :(S ₆)	6.60	5.05	-8.93	6.10	-2.53	2.60	890	33,34
C-Sc ₂ O ₃ :(C ₂)	6.60	5.02	-8.90	6.30	-2.28	2.54	950	33
La ₂ O ₂ S	6.37	3.64	-7.41	4.75	-2.48	1.37	400	19,35
Y ₂ O ₂ S	6.37	3.76	-7.53	4.85	-2.49	1.47	460	19
KLuS ₂	6.20	3.02	-6.71	4.35	-2.21	0.81	150	36
YSiO ₂ N	6.70	3.89	-7.81	6.10	-1.41	1.58	425	37
AlN-wurtzite	6.40	3.49	-7.27	6.20	-0.76	1.22	300	38
GaN-wurtzite	6.40	3.25	-7.03	3.48	-3.45	1.04	200	38-40

in relaxation effects, and the experimental errors in E^{CT} and T_{10} then provide the scatter of data.

Note that the fitted line does not cross the horizontal at zero energy but near 0.5 eV. We assumed that quenching occurs by the full ionization of the hole. However, this is not necessarily needed. The CT-state is a hole at the valence band that is still Coulomb bonded with the transferred electron, *i.e.*, Eu^{2+} , and radiation less recombination may start from this bonded state which will lower ΔE . Furthermore, 0.5 eV is of the same magnitude as the energy involved in lattice relaxation and Stokes shift.^{15,41} We therefore interpret the intercept near 0.5 eV as an effect of electron-hole bonding and lattice relaxation.

B. Thermal quenching of the $\text{Tb}^{3+} ^5\text{D}_4$ emission

The energy gap between the emitting $^5\text{D}_4$ level of Tb^{3+} and the next lower $^7\text{F}_0$ 4f^8 -level is about 1.8 eV. This is even larger than that in the case of Eu^{3+} considered above, and multi-phonon relaxation is like for Eu^{3+} not a feasible quenching mechanism. Instead, in cases where the CB-bottom is not too far above the $^5\text{D}_4$ level, thermal quenching can proceed by electron ionization to the CB. For YPO_4 in Fig. 3 with the CB-bottom at -0.63 eV, the distance is 4.5 eV which is clearly too large. However, in transition metal based compounds like tantalates, tungstates, vanadates, niobates, molybdates and titanates, the CB-bottom appears at -3 eV to -4 eV.⁴² The excitation spectra

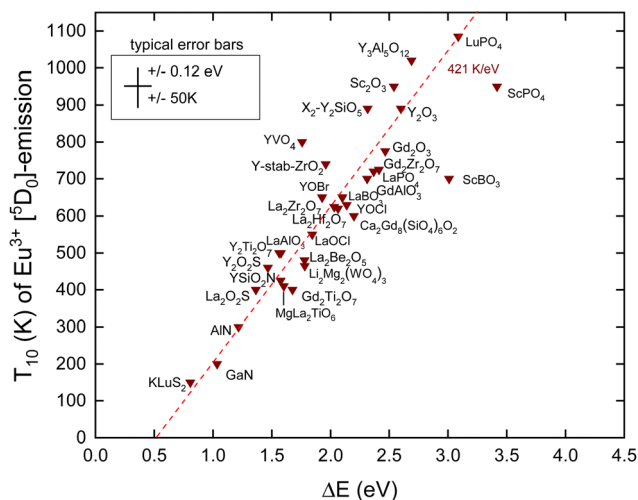


Fig. 4 10% Quenching temperature T_{10} for the Eu^{3+} emission from the $^5\text{D}_0$ level against the energy difference between the $^5\text{D}_0$ hole state and the VB-top. The fitted dashed line has a slope of 421 K eV^{-1} .



of the Tb^{3+} emission in these compounds often reveal a so-called intervalence charge transfer (IVCT) band attributed to the excitation of an electron from the $Tb^{3+} 7F_6$ ground state^{43,44} to the CB. Whereas the CT-band energy of Eu^{3+} provides the location of the Eu^{2+} ground state above the VB, the IVCT band provides the Tb^{3+} ground state below the CB. Therefore, the IVCT band energy determines the quenching energy barrier ΔE and therewith the quenching temperature T_{50} . This was already demonstrated for Tb^{3+} in transition metal element based compounds in ref. 42. In ref. 14, compounds such as SnO_2 , Ga_2O_3 , Lu_2O_3 , and GaN with low lying conduction bands were added to the collection.

IVCT bands are ≈ 0.8 eV broad and in many compounds they tend to overlap partly with the host excitation band. This introduces often larger errors in the derived value for the IVCT energy $E^{IVCT}(Tb^{3+})$. To improve accuracy, one may construct a VRBE diagram as shown in Fig. 3 that combines the spectroscopic data on many different lanthanides thus leading to more accurate ΔE values. This method was followed in ref. 14 and 42 where VRBE diagrams were constructed using the 2012 chemical shift model.⁸ We will adopt here the same method but now using the refined chemical shift model which provides few 0.1 eV different $Tb^{4+/3+}$ CTL energies. The results are compiled in Table 3 and are shown in Fig. 5. Other than for Eu^{3+} , there is no need to correct for bandgap lowering with the increase of temperature because we assume that the Tb^{3+} levels move down with the same pace as the downward movement of the CB-bottom.

When assuming that the energy E^{IVCT} at the maximum of the IVCT band locates the Tb^{3+} ground state below the CB-bottom, one obtains for ΔE

$$\Delta E = E^{IVCT}(Tb^{3+}) - E(^5D_4) \quad (6)$$

where $E(^5D_4) = 2.55$ eV is the energy of the 5D_4 level above the ground state and the values on $E^{IVCT}(Tb^{3+})$ can be found in ref. 62.

Table 3 T_{50} data for emission from the 5D_4 level of Tb^{3+} in compounds against the energy difference ΔE between the 5D_4 level and the CB-bottom. The parameters used for the VRBE-diagram construction are provided. All energies are in eV

A	U	E^{CT}	E_V	E^{ex}	E_C	ΔE	T_{50}	Ref.
SnO_2	7.00	3.85	-7.92	3.59	-4.23	0.79	190	45
$CaSnO_3$	6.80	4.37	-8.34	4.93	-3.21	1.55	420	46
$\beta-Ga_2O_3$	6.90	4.28	-8.40	5.05	-3.15	1.80	385	47
$CaMoO_4$	7.00	4.40	-8.47	4.60	-3.70	1.32	450	48
$KLa(MoO_4)_2$	7.05	4.20	-8.29	4.60	-3.52	1.56	455	49
$KY(WO_4)_2$	7.15	4.60	-8.74	4.55	-4.03	1.18	410	50
$KLu(WO_4)_2$	7.15	4.55	-8.69	4.50	-4.03	1.18	325	51
$LaVO_4$	6.80	3.95	-7.92	4.25	-3.53	1.24	230	52
$GdVO_4$	6.84	4.05	-8.04	4.00	-3.91	0.90	140	53
$LuVO_4$	6.80	4.06	-8.03	3.85	-4.06	0.70	80	53
$LiNbO_3$	6.87	4.47	-8.47	4.62	-3.68	1.17	200	54,55
$CaNb_2O_6$	6.85	4.10	-8.10	4.75	-3.16	1.66	490	56
$YNbO_4$	6.84	4.60	-8.59	4.96	-3.43	1.38	455	56
$LiTaO_3$	6.65	4.54	-8.44	5.50	-2.70	1.87	585	55
$M'-YTbO_4$	6.78	5.10	-9.06	5.95	-2.83	1.91	750	57
$C-Lu_2O_3:(C_2)$	6.60	4.81	-8.69	5.90	-2.51	2.00	525	58
$Ga_{0.7}Al_{0.3}N$	6.40	3.22	-7.01	4.05	-2.83	1.44	250	59
GaN -wurtzite	6.40	3.25	-7.03	3.48	-3.45	0.81	30	59-61

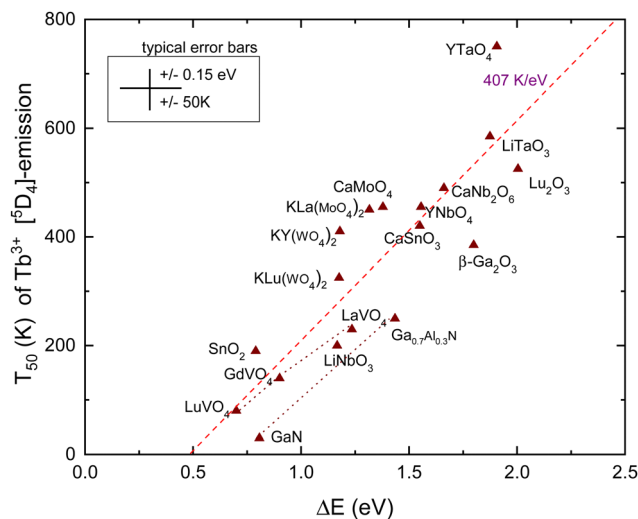


Fig. 5 T_{50} data for emission from the 5D_4 level of Tb^{3+} in compounds against the energy difference ΔE between the 5D_4 level and the CB-bottom.

When the quenching energy barrier is derived from the VRBE diagram construction one obtains for ΔE

$$\Delta E = [E^{ex} + 0.008(E^{ex})^2] - [E^{CT} - U + \Delta E(Eu, Tb) + E(^5D_4)] \quad (7)$$

where the first term between square brackets is the energy of the CB-bottom with respect to the VB-top and the second term of the 5D_4 state with respect to the VB-top where $\Delta E(Eu, Tb) \approx 3.5$ eV is the slightly compound dependent energy difference between the Eu^{3+} and Tb^{3+} ground state energies. The energy E^{CT} is not necessarily experimentally determined from the energy of the Eu^{3+} CT-band. It is often deduced from the constructed VRBE schemes that can be based, e.g., on CT-bands other than that of Eu^{3+} , experimental IVCT energies, or photoelectron spectroscopy data.

The dashed line in Fig. 5 is from a linear least squares fit through the data and has a slope of 407 K eV^{-1} . This is somewhat smaller than the value of 475 K eV^{-1} predicted in Table 1. Nevertheless, a clear correspondence between the quenching temperature and the energy at the CB-bottom is evident. The situation and figure much resemble that of hole ionization in the case of Eu^{3+} as shown in Fig. 4. The similar lifetimes of 1–2 ms for Eu^{3+} and Tb^{3+} emissions result in similar slopes in the linear fits. Also, the intersection with the horizontal axis for both dopants occurs near 0.5 eV.

Note that the 5D_3 level of Tb^{3+} is located 0.7 eV above the 5D_4 level and therefore located 0.7 eV closer to the CB-bottom. Since the 5D_3 and 5D_4 lifetimes differ not too much (factor of 2), one may expect about 350 K lower thermal stability of the 5D_3 emission. Indeed, the difference amounts 375 K for $CaMoO_4$ ⁶³ and 370 K for $CaNb_2O_6$.⁵⁶ Furthermore, whenever $T_{50}(^5D_4) < 300$ K, the emission from 4D_3 is absent even down to 4 K. This can be verified with the data compiled in ref. 42.

C. Thermal quenching of the $Pr^{3+} 3P_0$ emission

The $Pr^{4+/3+}$ CTL is near the same energy as that for $Tb^{4+/3+}$. Also, the emitting 3P_0 level of Pr^{3+} is near the same VRBE as that for



the 5D_4 level of Tb^{3+} as can be seen in the scheme for YPO_4 in Fig. 3. This means that like for Tb^{3+} thermal quenching may proceed by electron ionization to the CB in compounds with the low lying CB-bottom. Other than Tb^{3+} and Eu^{3+} , the next lower excited state (1D_2) is only at $\Delta E_{mp} = 0.5$ eV lower energy. At a sufficiently high temperature, the multi-phonon relaxation to 1D_2 then becomes also a possible quenching route. The radiative lifetime of the 3P_0 state is usually between 10 and 50 μs and is therefore shorter than those of Eu^{3+} and Tb^{3+} . This translates to a steeper $T_{50}/\Delta E = 560$ K eV^{-1} slope as shown in Table 1. In ref. 42, a relationship between T_{50} of the 3P_0 emission and the energy of the IVCT band, or equivalently the energy distance from the CB-bottom, was already demonstrated. Since then, more data have become available. Here, we have re-analyzed everything with the refined chemical shift model. The results are shown in Fig. 6 and compiled in Table 4.

For the quenching energy barrier, we used the same method as for Tb^{3+} . When assuming that the energy $E^{IVCT}(Pr^{3+})$ at the maximum of the IVCT band locates the Pr^{3+} ground state below the CB-bottom one obtains for ΔE

$$\Delta E = E^{IVCT}(Pr^{3+}) - E(^3P_0) \quad (8)$$

where $E(^3P_0) = 2.55$ eV is the energy of the 3P_0 level above the ground state and the values on $E^{IVCT}(Pr^{3+})$ can be found in ref. 62.

When the quenching energy barrier is derived from the VRBE construction one obtains for ΔE

$$\Delta E = [E^{ex} + 0.008(E^{ex})^2] - [E^{CT} - U + \Delta E(Eu, Pr) + E(^3P_0)] \quad (9)$$

where $\Delta E(Eu, Pr) \approx 3.49$ eV is the energy difference between the Eu^{3+} and Pr^{3+} ground state energies.

The dashed line drawn through the data has a slope of 560 K eV^{-1} as predicted from Table 1. It crosses the horizontal axis near 0.3 eV which compares with that for Tb^{3+} and Eu^{3+}

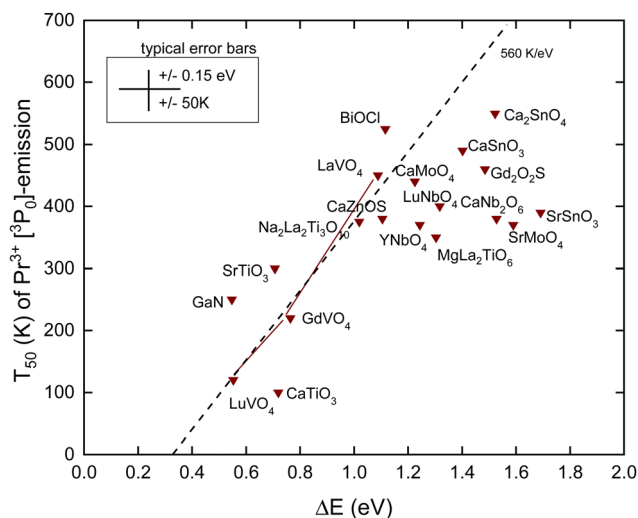


Fig. 6 T_{50} data for the emission from the 3P_0 level of Pr^{3+} in compounds against the energy difference ΔE between the 3P_0 level and the conduction band bottom.

Table 4 T_{50} data for emission from the 3P_0 level of Pr^{3+} in compounds against the energy difference between the 3P_0 level and the CB-bottom. The parameters used for the VRBE-diagram construction are provided. All energies are in eV

A	U	E^{CT}	E_V	E^{ex}	E_C	ΔE	T_{50}	Ref.
BiOCl	6.70	3.55	-7.47	4.00	-3.34	1.12	525	64
SrSnO ₃	6.96	4.00	-8.05	4.70	-3.17	1.69	390	65
CaSnO ₃	6.80	4.37	-8.34	4.93	-3.21	1.40	490	65
Ca ₂ SnO ₄	6.85	4.43	-8.42	5.05	-3.17	1.52	550	65
SrMoO ₄	7.05	4.25	-8.34	4.75	-3.41	1.59	≈ 370	66
CaMoO ₄	7.00	4.40	-8.47	4.60	-3.70	1.23	440	67
LaVO ₄	6.80	3.95	-7.92	4.25	-3.53	1.09	450	44
GdVO ₄	6.84	4.05	-8.04	4.00	-3.91	0.76	220	53
LuVO ₄	6.80	4.06	-8.03	3.85	-4.06	0.55	120	53
CaNb ₂ O ₆	6.85	4.10	-8.10	4.75	-3.16	1.53	380	56
YNbO ₄	6.84	4.60	-8.59	4.96	-3.43	1.24	370	56
LuNbO ₄	6.85	4.58	-8.58	5.00	-3.38	1.32	400	68
SrTiO ₃	6.75	3.44	-7.39	3.46	-3.83	0.71	≈ 300	69,70
CaTiO ₃	6.75	3.84	-7.79	3.85	-3.82	0.72	≈ 100	69,70
Na ₂ La ₂ Ti ₃ O ₁₀	6.75	3.70	-7.65	4.00	-3.52	1.02	375	71
MgLa ₂ TiO ₆	6.68	3.88	-7.79	4.50	-3.13	1.30	350	72
CaZnOS	6.35	3.73	-7.49	4.51	-2.82	1.11	380	73
Gd ₂ O ₂ S	6.37	3.72	-7.49	4.83	-2.47	1.49	460	74
GaN-wurtzite	6.40	3.25	-7.03	3.48	-3.45	0.55	250	75,76

where the crossing was near 0.5 eV. The data seem initially to follow this slope, but when T_{50} approaches 400 K many data points start to level off. The mentioned multi-phonon relaxation to the 1D_0 level may be responsible for this. A detailed analysis for each compound would be required to resolve this further. It is interesting to compare the results for the sequence of compounds $LaVO_4$, $GdVO_4$, and $LuVO_4$ where the bottom of the CB-band is formed by the lowest 3d-orbitals of V^{4+} .⁴² In this sequence, this CB-bottom lowers by about 0.5 eV, see column 6 in Tables 3 and 4. For both the Tb^{3+} 5D_4 emission and the Pr^{3+} 3P_0 emission, this leads to increasingly lower T_{50} as seen in Fig. 5 and 6.

The 1G_4 level of Pr^{3+} is $\Delta E_{mp} = 0.86$ eV below the 1D_2 level which makes multi-phonon relaxation from 1D_2 less probable than that from the 3P_0 level. The quenching of the 1D_2 emission may again proceed *via* the CB. Although the lifetime of the 1D_2 level is about 10 times longer than that of 3P_0 its 0.5 eV further distance below the CB is more important leading to the significantly higher thermal stability of the 1D_2 emission. The difference in T_{50} for $CaNb_2O_6$,⁵⁶ $LuNbO_4$,⁶⁸ and $MgLa_2TiO_6$ ⁷² appears about 200 K in line with the expectation.

D. Thermal quenching of the Eu^{2+} $4f^6$ $5d-4f^7$ emission

Techniques such as photoconductivity, excited state absorption, delayed fluorescence, and thermoluminescence charging studies have evidenced that the quenching of the Eu^{2+} emission proceeds often, if not always, by means of the thermal ionization of the 5d electron to the CB. The consistency between quenching *via* the CB and Eu^{2+} level locations with respect to the CB-bottom was demonstrated in ref. 77. The same was concluded from first principles studies on fifteen representative Eu^{2+} -doped phosphors by Jia *et al.*⁷⁸

The nature of the 5d-4f emission is much different from that of the $4f^n-4f^n$ emission. The transition is dipole allowed



Table 5 T_{50} data for the Eu^{2+} 5d–4f emission in compounds (A) against the energy difference between the lowest energy of the relaxed 4f⁶ 5d level and the CB-bottom. The parameters used for the VRBE-diagram construction are provided. All energies are in eV

A	U	E^{CT}	E_{V}	E^{ex}	E_{C}	E_{fd}	ΔS	ΔE	T_{50}	Ref.
RbCl ^a	6.70	4.20	−8.12	7.54	−0.13	3.19	0.21	1.01	670	83
KCl ^a	6.70	4.23	−8.15	7.79	0.12	3.10	0.17	1.16	770	83
NaCl ^a	6.70	4.48	−8.40	7.96	0.06	3.02	0.12	1.15	850	83
RbBr ^a	6.60	3.10	−6.98	6.64	0.02	3.16	0.17	1.02	690	83
KBr ^a	6.60	3.53	−7.41	6.80	−0.24	3.14	0.22	1.14	717	83
NaBr ^a	6.60	3.40	−7.28	6.75	−0.16	3.02	0.13	0.96	740	83
CsI ^a	6.25	2.60	−6.31	5.80	−0.24	2.97	0.19	0.50	220	84
KI ^a	6.25	3.00	−6.71	5.88	−0.56	3.07	0.20	0.99	450	85
Ba ₅ (PO ₄) ₃ Cl	6.89	4.40	−8.41	7.30	−0.69	3.05	0.20	0.37	510	86,87
Sr ₅ (PO ₄) ₃ Cl	6.90	4.66	−8.68	7.50	−0.73	2.92	0.15	0.45	460	88
Ca ₅ (PO ₄) ₃ Cl	6.88	5.04	−9.05	7.70	−0.88	2.97	0.24	0.28	480	87,89
Ca ₂ BO ₃ Cl	6.77	4.49	−8.45	7.15	−0.89	2.68	0.43	0.60	450	90
Ca ₈ Mg(SiO ₄) ₄ Cl ₂	6.60	4.47	−8.35	6.95	−1.01	2.61	0.16	0.34	425	91
α-Sr ₂ P ₂ O ₇	7.13	4.68	−8.81	7.85	−0.47	3.12	0.16	0.62	470	92
LiSrPO ₄	7.05	4.77	−8.86	7.75	−0.63	2.95	0.20	0.61	450	93
Ca ₁₀ K(PO ₄) ₇	7.05	5.06	−9.15	8.00	−0.64	2.95	0.27	0.64	450	94
NaCaPO ₄	7.07	4.77	−8.87	7.75	−0.64	2.77	0.31	0.85	600	95,96
YPO ₄	7.09	5.65	−9.77	8.55	−0.63	2.94	0.04	0.57	230	97
LuPO ₄	7.08	5.74	−9.85	8.70	−0.55	2.94	0.05	0.65	230	97
BaB ₈ O ₁₃	7.30	5.15	−9.38	8.15	−0.69	3.35	0.24	0.30	500	98,99
SrB ₆ O ₁₀	7.31	5.49	−9.71	8.30	−0.86	3.35	0.15	0.08	300	100
Ba ₂ Ca(BO ₃) ₂	6.93	4.61	−8.64	6.90	−1.36	2.79	0.38	0.07	190	101
NaBa ₄ (BO ₃) ₃	6.84	4.58	−8.57	7.00	−1.18	2.64	0.35	0.35	280	102
NaSr ₄ (BO ₃) ₃	6.85	4.65	−8.64	7.20	−1.03	2.67	0.69	0.64	370	102
BaBPO ₅	7.24	4.81	−9.00	8.53	0.12	3.42	0.16	0.97	565	103
SrBPO ₅	7.22	4.96	−9.14	8.53	−0.03	3.49	0.29	0.80	450	103
α-CaAl ₂ B ₂ O ₇	7.03	4.96	−9.04	7.30	−1.32	3.06	0.18	−0.21	60	104
CaBPO ₅	7.22	5.06	−9.24	8.55	−0.11	3.31	0.23	0.88	265	103
α-SrSiO ₃	6.63	5.04	−8.93	7.70	−0.76	3.02	0.21	0.21	130	105
CaMgSi ₂ O ₆	7.03	5.10	−9.18	7.95	−0.73	2.97	0.20	0.49	390	106
Ba ₂ MgSi ₂ O ₇	6.95	4.34	−8.38	7.00	−0.99	2.84	0.37	0.40	460	107,108
Sr ₂ MgSi ₂ O ₇	7.03	4.75	−8.83	7.29	−1.12	2.82	0.19	0.24	250	109,110
BaCa ₂ Mg(SiO ₄) ₂	6.90	4.20	−8.22	7.85	0.12	3.31	0.42	1.05	530	111,112
Ba ₂ SiO ₄	6.87	4.35	−8.36	7.05	−0.91	2.70	0.24	0.52	420	113–115
Sr ₃ Mg(SiO ₄) ₂	6.91	4.54	−8.57	7.45	−0.67	3.02	0.32	0.49	515	116
Sr ₂ SiO ₄	6.81	4.64	−8.61	7.20	−1.00	3.19	0.55	0.07	425	117
Li ₂ SrSiO ₄	6.91	4.81	−8.83	7.12	−1.30	2.43	0.26	0.42	525	118
CaAl ₂ (SiO ₄) ₂	6.95	4.44	−8.48	7.50	−0.53	3.08	0.19	0.53	480	119
Ca ₃ Mg(SiO ₄) ₂	6.86	4.96	−8.96	7.60	−0.90	3.02	0.41	0.28	435	116,120
β-Ca ₂ SiO ₄	6.80	4.77	−8.74	7.25	−1.07	2.86	0.41	0.24	390	107
Li ₂ CaSiO ₄	6.92	4.77	−8.80	7.55	−0.79	2.73	0.14	0.58	450	121
Sr ₃ SiO ₅	6.74	4.07	−8.01	6.50	−1.17	2.43	0.29	0.48	485	122
BaAl ₂ O ₄	6.82	4.63	−8.61	7.20	−1.00	2.92	0.44	0.29	270	123,124
Sr ₂ Al(AlSiO ₇)	6.82	4.79	−8.77	7.50	−0.82	2.88	0.23	0.39	300	125
SrAl ₁₂ O ₁₉	7.06	4.75	−8.85	8.00	−0.33	3.54	0.43	0.43	375	126
SrAl ₄ O ₇	6.89	5.02	−9.03	8.00	−0.52	3.10	0.47	0.63	260	126
SrAl ₂ O ₄ :(site 2)	6.80	4.55	−8.52	6.85	−1.30	3.06	0.28	−0.25	210	127,128
SrAl ₂ O ₄ :(site 3)	6.80	4.19	−8.16	6.85	−0.94	2.76	0.37	0.46	420	127,128
Sr ₄ Al ₁₄ O ₂₅ :[HE-site]	7.10	4.77	−8.89	7.70	−0.72	3.49	0.44	0.13	400	129
Sr ₄ Al ₁₄ O ₂₅ :[LE-site]	6.85	4.77	−8.77	7.70	−0.59	2.82	0.30	0.73	380	129
Ca ₂ Al(AlSiO ₇)	6.83	4.98	−8.97	7.60	−0.90	2.58	0.24	0.62	340	130,131
CaAl ₂ O ₄	6.80	4.73	−8.70	7.40	−0.86	3.14	0.32	0.13	320	132,133
CaO	6.31	4.88	−8.62	6.94	−1.30	1.89	0.21	0.66	250	134
Ca ₂ SiS ₄	6.40	2.06	−5.84	5.00	−0.64	2.38	0.18	0.85	445	135
SrGa ₂ S ₄	6.30	1.87	−5.61	4.77	−0.65	2.55	0.23	0.65	470	136,137
CaGa ₂ S ₄	6.25	1.90	−5.61	4.52	−0.93	2.36	0.14	0.49	450	138
CaS	6.17	2.35	−6.03	4.70	−1.15	2.07	0.16	0.54	475	139
SrSi ₂ O ₂ N ₂	6.70	3.44	−7.36	6.35	−0.69	2.51	0.21	0.83	600	81
SrSi ₂ AlO ₂ N ₃	6.60	2.97	−6.85	5.60	−0.99	2.73	0.23	0.27	450	140
CaSi ₂ O ₂ N ₂	6.70	3.10	−7.02	6.30	−0.41	2.56	0.33	1.13	455	81
Sr ₂ Si ₅ N ₈	6.33	2.56	−6.31	5.00	−1.11	2.19	0.18	0.53	550	141
Ca ₂ Si ₅ N ₈	6.35	2.93	−6.69	5.15	−1.33	2.27	0.21	0.26	370	142
CaAlSiN ₃	6.22	2.64	−6.34	5.05	−1.09	2.14	0.23	0.59	640	143,144
SrMg ₂ Al ₂ N ₄	6.15	2.21	−5.88	4.10	−1.64	2.13	0.12	−0.05	290	145

^a For the alkaline halides, the spectroscopic data on E^{CT} are not available. The values listed are the energy differences between the $\text{Eu}^{3+/2+}$ CTLs and E_{V} that was obtained directly from the published photoelectron spectroscopy data.



Table 6 T_{50} data for the $Ce^{3+} 5d-4f$ emission in compounds (A) against the energy difference between the lowest energy of the relaxed 5d level and the CB-bottom. The parameters used for the VRBE-diagram construction are provided. All energies are in eV

A	U	E^{CT}	E_V	E^{ex}	E_C	E_{fd}	ΔS	ΔE	T_{50}	Ref.
BaF ₂	7.38	7.67	-11.9	10.10	-1.02	4.25	0.19	1.01	400	146-148
SrF ₂	7.32	7.90	-12.1	10.60	-0.64	4.17	0.15	1.36	490	146
CaF ₂	7.31	8.21	-12.4	11.10	-0.35	4.04	0.09	1.73	620	11
LaF ₃	7.51	7.43	-11.8	10.45	-0.44	4.98	0.64	1.29	450	11
LiYF ₄	7.52	8.09	-12.4	11.00	-0.46	4.32	0.19	1.72	1025	11
LaBr ₃	6.60	2.00	-5.87	5.40	-0.24	4.07	0.54	0.94	750	149
YI ₃	6.29	1.48	-5.21	4.45	-0.60	3.07	0.60	1.14	650	150
Sr ₃ (Al ₂ O ₅)Cl ₂	6.77	4.51	-8.47	6.70	-1.41	3.70	0.75	0.51	525	151
LaOBr	6.58	4.11	-7.98	6.25	-1.41	3.47	0.43	0.28	300	152,153
GdOBr	6.56	4.24	-8.10	6.40	-1.37	3.34	0.26	0.34	450	153
LaP ₃ O ₉	7.26	5.84	-10.0	8.45	-1.02	4.28	0.21	0.80	690	154
LiYP ₄ O ₁₂	7.26	6.17	-10.4	8.63	-1.15	4.19	0.21	0.77	700	155
YPO ₄	7.09	5.65	-9.77	8.55	-0.63	3.85	0.13	1.32	725	156
Ca ₉ Y(PO ₄) ₇	7.08	4.86	-8.97	7.40	-1.13	4.31	0.68	0.62	600	157
Ba ₂ Ca(BO ₃) ₂	6.90	4.61	-8.63	6.90	-1.35	3.14	0.49	1.20	550	158
LiSr ₄ (BO ₃) ₃	6.89	4.66	-8.67	7.04	-1.24	3.73	0.75	0.82	525	159
Li ₆ Gd(BO ₃) ₃	6.98	4.88	-8.94	7.10	-1.44	3.59	0.36	0.71	310	160,161
Li ₆ Y(BO ₃) ₃	6.98	4.98	-9.04	7.20	-1.42	3.58	0.39	0.75	440	162
La ₂ Si ₂ O ₇	6.95	5.54	-9.58	7.45	-1.69	3.79	0.29	0.18	625	163
Gd ₂ Si ₂ O ₇	6.64	4.92	-8.81	7.20	-1.20	3.53	0.38	0.50	520	164,165
Lu ₂ Si ₂ O ₇	7.01	5.50	-9.57	7.30	-1.85	3.54	0.29	0.36	500	166-168
CaAl ₂ (SiO ₄) ₂	6.95	4.44	-8.48	7.50	-0.53	4.22	0.43	0.98	635	169
LiYSiO ₄	6.89	5.51	-9.52	7.55	-1.52	3.55	0.44	0.57	600	170
Ca ₃ Sc ₂ Si ₃ O ₁₂	6.85	5.15	-9.14	7.20	-1.53	2.77	0.34	1.24	1150	171,172
LaBO(SiO ₄)	7.03	4.84	-8.92	7.80	-0.64	4.34	0.46	0.90	600	173
La ₅ (SiO ₄) ₂ BO ₄ O	6.84	4.38	-8.37	6.70	-1.31	3.57	0.59	0.76	395	174
X1-Gd ₂ SiO ₅ :(Ce1)	6.85	4.90	-8.90	6.80	-1.73	3.61	0.70	0.37	350	175,176
X1-Gd ₂ SiO ₅ :(Ce2)	6.85	4.90	-8.90	6.80	-1.73	3.32	0.69	0.67	250	175,176
X2-Y ₂ SiO ₅ :(Ce1)	6.86	4.80	-8.80	6.82	-1.61	3.45	0.31	0.47	440	177,178
X2-Y ₂ SiO ₅ :(Ce2)	6.80	4.81	-8.78	6.82	-1.59	3.25	0.67	0.78	410	178
X2-Lu ₂ SiO ₅ :(Ce1)	6.83	5.15	-9.14	6.85	-1.91	3.46	0.31	0.11	350	178,179
X2-Lu ₂ SiO ₅ :(Ce2)	6.83	5.15	-9.14	6.85	-1.91	3.36	0.68	0.40	290	178,179
Sr ₃ Y ₂ Ge ₃ O ₁₂	6.85	4.43	-8.43	5.96	-2.18	2.86	0.38	0.51	300	172,180
Ca ₃ Y ₂ Ge ₃ O ₁₂	6.85	4.77	-8.77	6.20	-2.26	2.92	0.36	0.37	265	180
Mg ₃ Y ₂ Ge ₃ O ₁₂	6.90	4.70	-8.72	6.00	-2.43	2.59	0.40	0.61	300	181
Sr ₂ Al(AlSiO ₇)	6.82	4.79	-8.77	7.50	-0.82	3.69	0.25	0.94	500	182
Ca ₂ Al(AlSiO ₇)	6.83	4.98	-8.97	7.60	-0.90	3.48	0.30	1.09	570	182
Gd ₃ Al ₅ O ₁₂	6.84	5.39	-9.38	6.55	-2.49	2.64	0.42	0.43	400	183,184
GdAlO ₃	6.75	4.75	-8.70	7.36	-0.90	4.09	0.37	0.41	345	185
Y ₄ Al ₂ O ₉	6.75	5.19	-9.13	6.45	-2.35	3.18	0.35	-0.14	60	186
Y ₃ Al ₅ O ₁₂	6.77	5.23	-9.19	7.10	-1.69	2.71	0.33	1.01	645	11,187,188
Y ₃ Sc ₂ Al ₃ O ₁₂	6.56	5.28	-9.14	6.90	-1.86	2.86	0.48	0.44	530	189
YAlO ₃	6.81	5.06	-9.04	8.00	-0.52	4.09	0.54	0.96	660	11,190
LuAlO ₃	6.83	5.30	-9.29	8.35	-0.38	4.03	0.51	1.18	850	190
Ca ₂ Ga(GaSiO ₇)	6.95	4.48	-8.52	5.85	-2.40	3.54	0.49	-0.18	450	191
Gd ₃ Ga ₁ Al ₄ O ₁₂	6.84	5.37	-9.36	6.50	-2.52	2.75	0.45	0.30	405	192,193
Gd ₃ Ga ₂ Al ₃ O ₁₂	6.86	5.28	-9.28	6.36	-2.59	2.81	0.47	0.21	405	192,193
Gd ₃ Ga ₃ Al ₂ O ₁₂	6.86	5.21	-9.21	6.29	-2.60	2.81	0.48	0.20	310	183,194,195
Gd ₃ Ga ₄ Al ₁ O ₁₂	6.88	5.00	-9.01	6.07	-2.65	2.88	0.49	0.12	150	193
Y ₃ Al ₄ GaO ₁₂	6.77	5.21	-9.17	7.10	-1.66	2.78	0.36	0.98	605	192,196
Y ₃ Al ₃ Ga ₂ O ₁₂	6.77	5.23	-9.19	6.93	-1.87	2.83	0.32	0.70	525	192,196
Y ₃ Al ₂ Ga ₃ O ₁₂	6.77	5.19	-9.14	6.52	-2.28	2.85	0.39	0.30	380	192,196
Y ₃ AlGa ₄ O ₁₂	6.80	5.12	-9.09	6.44	-2.32	2.93	0.45	0.26	275	192,196
Y ₃ Ga ₅ O ₁₂	6.85	5.05	-9.05	6.10	-2.65	2.90	0.35	-0.01	100	197,198
SrHfO ₃	6.62	4.40	-8.28	6.35	-1.61	4.07	0.84	-0.25	285	199
CaHfO ₃	6.64	4.51	-8.40	6.95	-1.07	3.71	0.77	0.65	360	200
LaLuO ₃	6.58	4.25	-8.11	6.35	-1.44	3.71	0.99	0.29	339	200
LaScO ₃	6.66	4.20	-8.10	6.20	-1.60	3.85	0.80	0.03	255	200
La ₂ Be ₂ O ₅	6.70	4.11	-8.03	6.28	-1.44	3.64	0.85	0.49	360	32
GdScO ₃	6.70	4.73	-8.65	6.10	-2.25	3.59	0.74	-0.34	232	200
CaSc ₂ O ₄	6.65	4.35	-8.25	6.35	-1.58	2.76	0.32	0.88	530	201,202
Y ₂ O ₂ S	6.37	3.76	-7.53	4.85	-2.49	2.68	0.65	-0.21	63	203
CaGa ₂ S ₄	6.25	1.90	-5.61	4.52	-0.93	2.92	0.26	0.74	575	204
LaSiO ₂ N	6.65	3.43	-7.33	5.65	-1.42	3.50	0.32	0.29	275	205
SrAlSi ₄ N ₇	6.40	2.88	-6.66	5.05	-1.41	2.80	0.42	0.69	525	206
La ₃ Si ₆ N ₁₁	6.50	3.04	-6.87	4.60	-2.10	2.72	0.36	0.19	525	207
LaSi ₃ N ₅	6.48	2.58	-6.40	4.85	-1.36	3.56	0.55	0.15	550	208



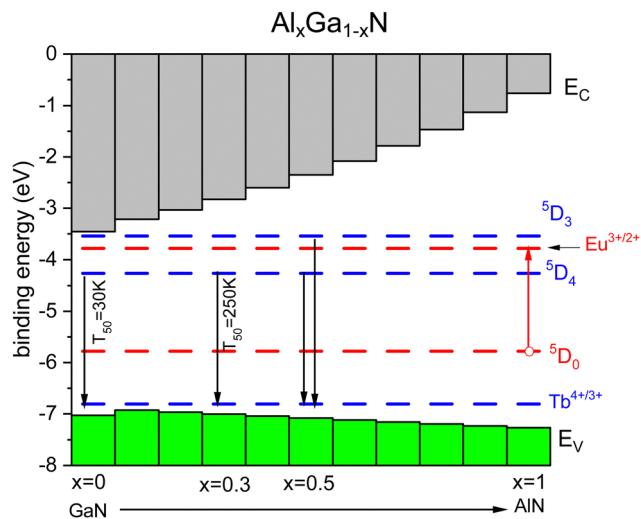


Fig. 9 Stacked VRBE scheme of the $\text{Al}_{1-x}\text{Ga}_x\text{N}$ system with the Tb^{3+} ground and excited state levels. The Eu^{3+} ground and excited 5D_0 levels are drawn as hole states.

With a slope relationship of 850 K eV^{-1} , 0.1 eV increase of the CB-bottom can already accomplish this increase. Lu^{3+} has a smaller ionic radius than Y^{3+} ; the lattice parameters decrease and the bandgap and CB-bottom increase upon introducing Lu. Incorporating larger lanthanides such as Gd^{3+} and La^{3+} would likewise reduce the quenching temperature. Indeed, the T_{50} of GdAlO_3 is only 345 K and for LaAlO_3 there is no Ce^{3+} emission because the 5d-level is located above the CB-bottom. This is all illustrated by the corresponding data points in Fig. 8.

The sensitivity of T_{50} on slight changes in the ΔE is also well demonstrated with Ce^{3+} doped $\text{Y}_3\text{Ga}_5\text{O}_{12}$. Depending on the synthesis temperature, part of the octahedral Ga^{3+} sites can be occupied by the larger Y^{3+} cations. This is known as the anti-site occupancy which leads to slight lattice expansion and band gap narrowing. In Czochralski grown crystals the Ce^{3+} emission is absent at 10 K^{197} but for powders grown with a relatively low temperature solid state synthesis there will be less anti-site occupancy, smaller lattice parameter, and wider bandgap. As a result the Ce^{3+} emission is observed at RT.¹⁹⁸

Fig. 3 shows that the VRBE in the lowest 5d-state of Pr^{3+} is about 0.5 eV below that for Ce^{3+} and similar will hold for other compounds. This implies that when quenching proceeds *via* the CB, the T_{50} for the $4f^15d-4f^2$ emission of Pr^{3+} should be about 400 K higher than that for Ce^{3+} . For BaF_2 indeed, the 5d-4f emission from Pr^{3+} is at least 200 K more stable than from Ce^{3+} .¹⁴⁶ However, the T_{50} values of Ce^{3+} and Pr^{3+} in $\text{Y}_3\text{Al}_{5-x}\text{Ga}_x\text{O}_{12}$ are 640 K and 321 K for $x = 0$, 583 K and 377 K for $x = 1$, 491 K and 407 K for $x = 2$, 344 K and 316 K for $x = 3$, and 301 K and 173 K for $x = 4$.^{196,215} For $x = 0, 1, 2, 3$, and 4, $T_{50}(\text{Ce})$ decreases because the 5d VRBE moves up and the CB-bottom moves down. However, $T_{50}(\text{Pr})$ increases for $x = 0, 1$, and 2 and this was attributed to quenching *via* the crossing point (CP) of the $4f^2$ [$^3\text{P}_2$] and $4f5d$ parabola's where the former remains stationary and the latter moves up with increasing x .²¹⁵ For $x = 3$ and 4, the CB moves down below the CP and both Ce and

Pr quench *via* the CB. The question remains though why $T_{50}(\text{Pr}) < T_{50}(\text{Ce})$ for $x = 3$ and $x = 4$. $T_{50}(\text{Pr}) < T_{50}(\text{Ce})$ was also observed in Y_2SiO_5 and Lu_2SiO_5 by van der Kolk *et al.*²¹⁶ where photocurrent studies did evidence quenching *via* the CB. It was suggested that the $^1\text{S}_0$ $4f^2$ level of Pr^{3+} located above the lowest energy $4f^1$ 5d-level assists in the quenching *via* the CB thus lowering T_{50} .²¹⁶ The final answer remains open and deserves a more dedicated study.

IV. Summary and conclusions

This work confirmed that the thermal quenching of Eu^{3+} , Tb^{3+} , Pr^{3+} , Eu^{2+} , and Ce^{3+} emissions proceeds *via* charge transfer to the host band states. By using a frequency factor of $2 \times 10^{13} \text{ Hz}$ and the typical value for the radiative lifetime of the emitting energy level, the rate of change in T_{50} with a quenching energy barrier ΔE was predicted as shown in Table 1. Using the refined chemical shift model for the VRBE diagram construction, the ΔE values of thermal quenching were derived. For the characteristic $4f^2-4f^2$ emissions of Eu^{3+} , Tb^{3+} , and Pr^{3+} , the predicted slopes $T_{50}/\Delta E$ (K eV^{-1}) were indeed observed. The 0.3–0.5 eV intercept with the horizontal in Fig. 4–6 was attributed partly to the relaxation energy accompanying the charge transfer and to the possibility/probability of quenching *via* the impurity trapped exciton state. The effect of relaxation is very compound dependent and is not accounted for in the VRBE diagram construction. When the quenching temperature is above 400 K for Pr^{3+} , it was suggested that multi-phonon relaxation from $^3\text{P}_0$ to $^1\text{D}_0$ becomes a dominating route for quenching.

The ΔE values for the 5d-4f emissions of Eu^{2+} and Ce^{3+} derived from VRBE diagrams carry substantial larger errors than those for Eu^{3+} , Tb^{3+} , and Pr^{3+} . This is due to the contribution from the error in E^{ex} , the Stokes ΔS and for Ce^{3+} also the U -value. These error sources are held responsible for the wide scatter of the the data points in Fig. 7 and 8. Nevertheless, clear trends are observed particularly when dealing with a sequence of a similar type of compounds like the garnet or rare earth perovskite family of compounds.

This work deals with about 170 different compounds, and for each of them all parameters needed to construct VRBE schemes like that for YPO_4 in Fig. 3 have been provided in various tables. This work has demonstrated that changes as small as 0.1 eV in level locations may already lead to a 50–100 K shift in T_{50} . Such changes can be accomplished by intentional or unintentional defects, the activator concentration, the occupation of anti-sites in garnets, and the application of pressure, synthesis conditions, *etc.* As a result, the often made assumption that ΔE in the Arrhenius equations is a constant will not hold for charge transfer quenching and then there is not much scientific sense in fitting a quenching curve with this Arrhenius equation. This work has also demonstrated the limitations of VRBE diagrams as shown in Fig. 3. (1) They do not deal with lattice relaxation effects leading to the very compound dependent Stokes shifts. (2) The assumption that the maximum of the



- 49 E. Cavalli, P. Boutinaud, T. Cucchiatti and M. Bettinelli, *Opt. Mater.*, 2009, **31**, 470.
- 50 S. Schwung, D. Rytz, B. Heying, U. C. Rodewald, O. Niehaus, D. Ensling, T. Justel and R. Pottgen, *J. Lumin.*, 2015, **166**, 289.
- 51 P. Boutinaud, M. Bettinelli and F. Diaz, *Opt. Mater.*, 2010, **32**, 1659.
- 52 A. H. Krumpel, E. van der Kolk, P. Dorenbos, P. Boutinaud, E. Cavalli and M. Bettinelli, *Mater. Sci. Eng., B*, 2008, **146**, 114.
- 53 A. H. Krumpel, E. van der Kolk, E. Cavalli, P. Boutinaud, M. Bettinelli and P. Dorenbos, *J. Phys.: Condens. Matter*, 2009, **21**, 115503.
- 54 W. Ryba-Romanowski, S. Golab, W. A. G. Dominiak-Dzik, M. N. Palatnikov and N. V. Sidorov, *Appl. Phys. Lett.*, 2001, **78**, 3610.
- 55 R. Lisiecki, B. Macalik, R. Kowalski, J. Komar and W. Ryba-Romanowski, *Crystals*, 2020, **10**, 1034.
- 56 P. Boutinaud, E. Cavalli and M. Bettinelli, *J. Phys.: Condens. Matter*, 2007, **19**, 386230.
- 57 G. Blasse and A. Brill, *J. Lumin.*, 1970, **3**, 109.
- 58 E. Zych and D. Kulesza, *Z. Naturforsch.*, 2014, **69b**, 165.
- 59 A. Wakahara, Y. Nakanishi, T. Fujiwara, A. Yoshida, T. Ohshima and T. Kamiya, *Phys. Status Solidi A*, 2005, **202**, 863.
- 60 Y. Nakanishi, A. Wakahara, H. Okada, A. Yoshida, T. Ohshima and H. Itoh, *Phys. Status Solidi B*, 2003, **240**, 372.
- 61 J. Rodrigues, M. Fialho, S. Magalhaes, M. R. Correia, L. Rino, E. Alves, A. J. Neves, K. Lorenz and T. Monteiro, *J. Lumin.*, 2016, **178**, 249.
- 62 P. Dorenbos, *Opt. Mater.*, 2019, **91**, 333.
- 63 E. Cavalli, A. Belletti, R. Mahiou and P. Boutinaud, *J. Lumin.*, 2010, **130**, 733.
- 64 Q. Wang, M. Xie, M. Fang, X. Wu, Y. Liu, Z. Huang, K. Xi and X. Min, *Molecules*, 2019, **24**, 1295.
- 65 A. Stanulis, A. Katelnikovas, M. VanBael, A. Hardy, A. Kareiva and T. Justel, *J. Lumin.*, 2016, **172**, 323.
- 66 L. Li, P. Yang, W. Xia, Y. Wang, F. Ling, Z. Cao, S. Jiang, G. Xiang, X. Zhou and Y. Wang, *Ceram. Int.*, 2021, **47**, 769.
- 67 E. Cavalli, F. Angiuli, P. Boutinaud and R. Mahiou, *J. Solid State Chem.*, 2012, **185**, 136.
- 68 C. Liu, F. Pan, Q. Peng, W. Zhou, R. Shi, L. Zhou, J. Zhang, J. Chen and H. Liang, *J. Phys. Chem. C*, 2016, **120**, 26044.
- 69 P. Boutinaud, L. Sarakha, R. Mahiou, E. Cavalli, M. Bettinelli, P. Dorenbos and R. Mahiou, *J. Phys. D: Appl. Phys.*, 2009, **42**, 045106.
- 70 S. Okamoto, H. Kobayashi and H. Yamamoto, *J. Appl. Phys.*, 1999, **86**, 5594.
- 71 Y. Wang, V. Tsiumra, Q. Peng, H. Liang, Y. Zhydachevskyy, M. Chaika, P. Dluzewski, H. Przybylinska and A. Suchocki, *J. Phys. Chem. A*, 2019, **123**, 4021.
- 72 R. Shi, L. Lin, P. Dorenbos and H. Liang, *J. Mater. Chem. C*, 2017, **5**, 10737.
- 73 X. Zhang, Q. Zhu, B. Chen, S. Wang, A. L. Rogach and F. Wang, *Adv. Photonics Research*, 2021, **2**, 2000089.
- 74 G. Blasse and A. Meijerink, *Inorg. Chim. Acta*, 1989, **160**, 29.
- 75 H. J. Lozykowski, W. M. Jadwisieniczak and I. Brown, *J. Appl. Phys.*, 2000, **88**, 210.
- 76 Y. E. Romanyuk, L. D. Kranz and S. R. Leone, *J. Appl. Phys.*, 2008, **103**, 073104.
- 77 P. Dorenbos, *J. Phys.: Condens. Matter*, 2005, **17**, 8103.
- 78 Y. Jia, A. Miglio, S. Ponce, M. Mikami and X. Gonze, *Phys. Rev. B: Condens. Matter Mater. Phys.*, 2017, **96**, 125132.
- 79 P. Dorenbos, *IEEE Trans. Nucl. Sci.*, 2010, **57**, 1162.
- 80 P. Dorenbos, *J. Lumin.*, 2003, **104**, 239.
- 81 V. Bachmann, C. Ronda, O. Oeckler, W. Schnick and A. Meijerink, *Chem. Mater.*, 2009, **21**, 316.
- 82 W. Drozdowski and A. J. Wojtowicz, *Nucl. Instrum. Methods Phys. Res., Sect. A*, 2002, **486**, 412.
- 83 G. Munoz, C. de la Cruz, A. Munoz and O. J. Rubio, *J. Mater. Sci. Lett.*, 1988, **7**, 1310.
- 84 V. Yakovlev, L. Trefilova, A. Meleshko and N. Ovcharenko, *J. Lumin.*, 2012, **132**, 2476.
- 85 F. Jaque, J. A. Hernandez, H. S. Murrieta and J. O. Rubio, *J. Phys. Soc. Jpn.*, 1982, **51**, 249.
- 86 P. Wang, J. Mao, X. Wei, L. Qiu, B. Jiang, F. Chi, M. Yina and Y. Chen, *J. Alloys and Comp.*, 2021, **869**, 159277.
- 87 Y. Wei, X. Qi, H. Xiao, W. Luo, H. Yao, L. Lv, G. Li and J. Lin, *RSC Adv.*, 2016, **6**, 43771.
- 88 A. Garcia, B. Latourrette and C. Fouassier, *J. Electrochem. Soc.: Sol. State Science and Techn.*, 1979, **126**, 1734.
- 89 J. Zheng, S. Wu, G. Chen, S. Dang, Y. Zhuang, Z. Guo, Y. Lu, Q. Cheng and C. Chen, *J. Alloys and Comp.*, 2016, **663**, 332.
- 90 Z. Xia, L. Liao, Z. Zhang and Y. Wang, *Mater. Res. Bull.*, 2012, **47**, 405.
- 91 J. Wang, M. Zhang, Q. Zhang, W. Ding and Q. Su, *Appl. Phys. B*, 2007, **87**, 249.
- 92 W. L. Wanmaker and J. W. ter Vrugt, *Phil. Res. Rept.*, 1967, **22**, 355.
- 93 G. B. Nair, H. C. Swart and S. J. Dhoble, *J. Lumin.*, 2019, **214**, 116564.
- 94 W.-R. Liu, Y.-C. Chiu, Y.-T. Yeh, S.-M. Jang and T.-M. Chen, *J. Electrochem. Soc.*, 2009, **156**, J169.
- 95 C. Qin, Y. Huang, L. Shi, G. Chen, X. Qiao and H. J. Seo, *J. Phys. D: Appl. Phys.*, 2009, **42**, 185105.
- 96 C. Zhao, Z. Xia and M. Li, *RSC Adv.*, 2014, **4**, 33114.
- 97 J. Zeler, M. Sulollari, A. Meijerink, M. Bettinelli and E. Zych, *J. Alloys Compd.*, 2020, **844**, 156096.
- 98 G. Blasse, A. Brill and J. de Vries, *J. Electrochem. Soc.: Sol. State Sci.*, 1968, **115**, 977.
- 99 Y. Xie, S. Zhang, Q. Zeng, Z. Pei and Q. Su, *J. Mater. Sci. Technol.*, 2004, **20**, 517.
- 100 M. Leskela, T. Koskentalo and G. Blasse, *J. Sol. St. Chem.*, 1985, **59**, 272.
- 101 A. Diaz and D. A. Keszler, *Chem. Mater.*, 1997, **9**, 2071.
- 102 J. Huang, J. Dai, D. Deng, H. Yu, Y. Li, Y. Hua, S. Zhao, C. Li and S. Xu, *RSC Adv.*, 2015, **5**, 85682.
- 103 G. Blasse, A. Brill and J. de Vries, *J. Inorg. Nucl. Chem.*, 1969, **31**, 568.
- 104 S. J. Camardello, P. J. Toscano, M. G. Brik and A. M. Srivastava, *Opt. Mater.*, 2014, **37**, 404.
- 105 S. H. M. Poort, H. M. Reijnhoudt, H. O. T. van der Kuip and G. Blasse, *J. Alloys Compd.*, 1996, **241**, 75.



- 106 F. Su, B. Lou, Y. Ou, Y. Yang, W. Zhou, C.-K. Duan and H. Liang, *J. Phys. Chem. C* **125**, 2021, 595.
- 107 G. Blasse, W. L. Wanmaker, J. W. ter Vrugt and A. Bril, *Philips Res. Rep.*, 1968, **23**, 189.
- 108 J. Yan, C. Liu, J. Vlieland, J. Zhou, P. Dorenbos, Y. Huang, Y. Tao and H. Liang, *J. Lumin.*, 2017, **183**, 97.
- 109 A. A. Setlur, A. M. Srivastava, L. Pham, M. Hannah and U. Happek, *J. Appl. Phys.*, 2008, **103**, 053513.
- 110 D. Jia, W. Jia and Y. Jia, *J. Appl. Phys.*, 2007, **101**, 023520.
- 111 D. Hou, C. Liu, X. Ding, X. Kuang, H. Liang, S. Sun, Y. Huang and Y. Tao, *J. Mater. Chem. C*, 2013, **1**, 493.
- 112 D. Hou, W. Chen, X. Ding, H. Liang, L. Zheng and J. Zhang, *ECS J. Solid State Sci. Technol.*, 2013, **2**, R79.
- 113 K. Asami, J. Ueda, K. Yasuda, K. Hongo, R. Maezono, M. G. Brik and S. Tanabe, *Opt. Mater.*, 2018, **84**, 436.
- 114 L. Lin, L. Ning, R. Zhou, C. Jiang, M. Peng, Y. Huang, J. Chen, Y. Huang, Y. Tao and H. Liang, *Inorg. Chem.*, 2018, **57**, 7090.
- 115 M. Yamaga, Y. Masui, S. Sakuta, N. Kodama and K. Kaminaga, *Phys. Rev. B: Condens. Matter Mater. Phys.*, 2005, **71**, 205102.
- 116 G. Blasse and A. Bril, *J. Chem. Phys.*, 1968, **48**, 217.
- 117 T. L. Barry, *ECS J. Solid State Sci. Technol.*, 1968, **115**, 1181.
- 118 S. S. B. Nasir, A. Tanaka, S. Yoshiara and A. Kato, *J. Lumin.*, 2019, **207**, 22.
- 119 T. J. Isaacs, *ECS J. Solid State Sci. Technol.*, 1971, **118**, 1009.
- 120 D. Stefanska and P. J. Deren, *Opt. Mater.*, 2018, **80**, 62.
- 121 J. Zhong, W. Zhao, L. Lan and J. Wang, *J. Mater. Sci.: Mater. Electron.*, 2014, **25**, 736.
- 122 Q. Shao, H. Lin, Y. Dong, Y. Fu, C. Liang, J. He and J. Jiang, *J. Solid State Chem.*, 2015, **225**, 72.
- 123 H. Aizawa, S. Komuro, T. Katsumata, S. Sato and T. Morikawa, *Thin Solid Films*, 2006, **496**, 179.
- 124 S. H. M. Poort, W. P. Blokpoel and G. Blasse, *Chem. Mater.*, 1995, **7**, 1547.
- 125 F.-C. Lu, L.-J. Bai, W. Dang, Z.-P. Yang and P. Lin, *ECS J. Solid State Sci. Technol.*, 2015, **4**, R27.
- 126 D. Dutczak, T. Justel, C. Ronda and A. Meijerink, *Phys. Chem. Chem. Phys.*, 2015, **17**, 15236.
- 127 J. Botterman, J. J. Joos and P. F. Smet, *Phys. Rev. B: Condens. Matter Mater. Phys.*, 2014, **90**, 085147.
- 128 J. Bierwagen, S. Yoon, N. Gartmann, B. Walfort and H. Hagemann, *Opt. Mater. Express*, 2016, **6**, 793.
- 129 D. Dutczak, C. Ronda, T. Justel and A. Meijerink, *J. Phys. Chem. A*, 2014, **118**, 1617.
- 130 Y. Luo and Z. Xia, *Opt. Mater.*, 2014, **36**, 1874.
- 131 T. Hu, Y. Gao, M. Molochev, Z. Xia and Q. Zhang, *Sci. China. Mater.*, 2019, **62**, 1807.
- 132 G. Blasse and A. Bril, *Philips Res. Rep.*, 1968, **23**, 201.
- 133 C. E. Tyner and H. G. Drickamer, *J. Chem. Phys.*, 1977, **67**, 4116.
- 134 S. H. M. Poort, A. Meyerink and G. Blasse, *J. Phys. Chem. Sol.*, 1997, **58**, 1451.
- 135 P. F. Smet, N. Avci and D. Poelman, *J. Electrochem. Soc.*, 2009, **156**, H243.
- 136 C. Chartier, C. Barthou, P. Benalloul and J. M. Frigerio, *J. Lumin.*, 2005, **111**, 147.
- 137 J. J. Joos, K. W. Meert, A. B. Parmentier, D. Poelman and P. F. Smet, *Opt. Mater.*, 2012, **34**, 1902.
- 138 P. Benalloul, C. Barthou, C. Fouassier, A. N. Georgobiani, L. S. Lepnev, Y. N. Emirov, A. N. Grutzintsev, B. G. Tagiev, O. B. Tagiev and R. B. Jabbarov, *J. Electrochem. Soc.*, 2003, **150**, G62.
- 139 M. Ando and Y. A. Ono, *J. Cryst. Growth*, 1992, **117**, 969.
- 140 V. Bachmann, A. Meijerink and C. Ronda, *J. Lumin.*, 2009, **129**, 1341.
- 141 R.-J. Xie, N. Hirosaki, N. Kimura, K. Sakuma and M. Mitomo, *Appl. Phys. Lett.*, 2007, **90**, 191101.
- 142 J. Li, B. Lei, J. Qin, Y. Liu and X. Liu, *J. Am. Ceram. Soc.*, 2013, **96**, 873.
- 143 J. Ueda, S. Tanabe, K. Takahashi, T. Takeda and N. Hirosaki, *Bull. Chem. Soc. Jpn.*, 2018, **91**, 173.
- 144 J. Tian, W. Zhuang, R. Liu, L. Wang, Y. Liu, C. Yan, G. Chen, H. Xu, M. Chen, Z. Jiang and X. Zhang, *J. Am. Ceram. Soc.*, 2019, **102**, 7336.
- 145 P. Pust, C. Hecht, V. Weiler, A. Locher, D. Zitnanska, S. Harm, D. Weichert, P. J. Schmidt and W. Schnick, *Chem. Mater.*, 2014, **26**, 6113.
- 146 R. Shendrik and E. Radzhabov, *IEEE Trans. Nucl. Sci.*, 2010, **57**, 1295.
- 147 P. Dorenbos, R. Visser, C. W. E. van Eijk, R. W. Hollander and H. W. den Hartog, *Nucl. Instrum. Methods*, 1991, **A310**, 236.
- 148 R. C. Tailor, O. H. Nestor and B. Utts, *IEEE TNS-33*, 1986, 243.
- 149 G. Bizarri, J. T. M. de Haas, P. Dorenbos and C. W. E. van Eijk, *Phys. Status Solidi A*, 2006, **203**, R41.
- 150 A. M. Srivastava, S. J. Camardello, H. A. Comanzo, M. Aycibin and U. Happek, *Opt. Mater.*, 2010, **32**, 936.
- 151 X. Zhang, B. Park, N. Choi, J. Kim, G. C. Kim and J. H. Yoo, *Mater. Lett.*, 2009, **63**, 700.
- 152 Z. Fu-Tan, C. Li-Yun and X. Xu-Rong, *ECS J. Solid State Sci. Technol.*, 1987, **134**, 3186.
- 153 D. M. de Leeuw, C. A. H. A. Mutsaers, H. Mulder and D. B. M. Klaasen, *ECS J. Solid State Sci. Technol.*, 1988, **135**, 1009.
- 154 P. Dorenbos, unpublished data.
- 155 T. Shalapska, G. Stryganyuka, D. Trotsch, T. Demkiv, A. Gektin, A. Voloshinovskii and P. Dorenbos, *J. Lumin.*, 2010, **130**, 1941.
- 156 T. Justel, P. Huppertz, W. Mayr and D. U. Wiechert, *J. Lumin.*, 2004, **106**, 225.
- 157 C.-H. Huang, T.-M. Chen and B.-M. Cheng, *Inorg. Chem.*, 2011, **50**, 6552.
- 158 H. Lin, H. Liang, Z. Tian, B. Han, J. Wang and Q. Su, *J. Phys. D: Appl. Phys.*, 2009, **42**, 165409.
- 159 Y. Yang, B. Lou, Y. Ou, F. Su, C.-G. Ma, C.-K. Duan, P. Dorenbos and H. Liang, *Inorg. Chem.*, 2022, **61**, 7654.
- 160 J. F. Chen, Y. Li, G.-L. Song, D.-M. Yao, L.-Y. Yuan, X.-J. Qi and S.-H. Wang, *J. Inorg. Mater.*, 2007, **22**(1), 25.
- 161 I. N. Ogorodnikov, N. E. Poryvai, I. N. Sedunova, A. V. Tolmachev and R. P. Yavetskiy, *Opt. Spectrosc.*, 2011, **110**, 266.



- 162 Y. Ou, W. Zhou, D. Hou, M. G. Brik, P. Dorenbos, Y. Huang and H. Liang, *RSC Adv.*, 2019, **9**, 7908.
- 163 Q. Wei, G. Liu, Z. Zhou, J. Wan, H. Yang and Q. Liu, *Mater. Lett.*, 2014, **126**, 178.
- 164 V. Jary, L. Havlak, J. Barta, E. Mihokova and M. Nikl, *IEEE Trans. Nucl. Sci.*, 2014, **61**, 385.
- 165 O. Sidletskiy, V. Baumer, I. Gerasymov, B. Grinyov, K. Katrunov, N. Starzhinsky, O. Tarasenko, V. Tarasov, S. Tkachenko, O. Voloshina and O. Zelenskaya, *Rad. Meas.*, 2010, **45**, 365.
- 166 V. Jary, M. Nikl, S. Kurosawa, Y. Shoji, E. Mihokova, A. Beitlerova, G. P. Pazzi and A. Yoshikawa, *J. Phys. Chem. C*, 2014, **118**, 26529.
- 167 L. Pidol, A. Kahn-Harari, B. Viana, B. Ferrand, P. Dorenbos, C. W. E. van Eijk and E. Virey, *J. Phys.: Cond. Matter.*, 2003, **15**, 2091.
- 168 H. Feng, D. Ding, H. Li, S. Lu, S. Pan, X. Chen and G. Ren, *J. Alloys Comp.*, 2011, **509**, 3855.
- 169 A. Pfahnl, *Bell Syst. Tech.*, 1963, 181.
- 170 R. Shi, J. Xu, G. Liu, X. Zhang, W. Zhou, F. Pan, Y. Huang, Y. Tao and H. Liang, *J. Phys. Chem. C*, 2016, **120**, 4529.
- 171 J. M. Herzog, D. Witkowski and D. A. Rothamer, *Meas. Sci. Technol.*, 2021, **32**, 054008.
- 172 S. K. Sharma, Y.-C. Lin, I. Carrasco, T. Tingberg, M. Bettinelli and M. Karlsson, *J. Mater. Chem. C*, 2018, **6**, 8923.
- 173 L. Zhou, W. Zhou, R. Shi, C. Liu, Y. Huang, Y. Tao and H. Liang, *J. Lumin.*, 2016, **177**, 178.
- 174 Z. Xia, M. S. Molochev, W. B. Im, S. Unithrattil and Q. Liu, *J. Phys. Chem. C*, 2015, **119**, 9488.
- 175 H. Suzuki, T. A. Tombrello, C. L. Melcher and J. S. Schweitzer, *IEEE Trans. Nucl. Sci.*, 1994, **41**, 681.
- 176 K. Mori, M. Nakayama and H. Nishimura, *Phys. Rev. B: Condens. Matter Mater. Phys.*, 2003, **67**, 165206.
- 177 E. Mihokova, K. Vavru, M. P. Horodysky, W. Chewpraditkul, V. Jary and M. Nikl, *IEEE Trans. on Nucl. Sci.*, 2012, **59**, 2085.
- 178 V. Jary, M. Nikl, E. Mihokova, J. A. Mares, P. Prusa, P. Horodysky, W. Chewpraditkul and A. Beitlerova, *IEEE Trans. Nucl. Sci.*, 2012, **59**, 2079.
- 179 J. D. Peak, C. J. Melcher and P. D. Rack, *J. Applied Phys.*, 2011, **110**, 013511.
- 180 H. Luo, L. Ning, Y. Dong, A. J. J. Bos and P. Dorenbos, *J. Phys. Chem. C*, 2016, **120**, 28743.
- 181 T. Shimizu, J. Ueda and S. Tanabe, *Phys. Stat. Sol. C*, 2012, **12**, 2296.
- 182 L. Lin, R. Shi, R. Zhou, Q. Peng, C. Liu, Y. Tao, Y. Huang, P. Dorenbos and H. Liang, *Inorg. Chem.*, 2017, **56**, 12476.
- 183 J. M. Ogieglo, A. Katelnikovas, A. Zych, T. Justel, A. Meijerink and C. R. Ronda, *J. Phys. Chem. A*, 2013, **117**, 2479.
- 184 I. V. Berezovskaya, A. S. Voloshinovskii, Z. A. Khapko, O. V. Khomenko, N. P. Eftyushina and V. P. Dotsenko, *Funct. Mater.*, 2021, **28**, 6.
- 185 E. van der Kolk, P. Dorenbos, J. T. M. de Haas and C. W. E. van Eijk, *Phys. Rev. B: Condens. Matter Mater. Phys.* **71**, 2005, 045121.
- 186 Y. Wang, R. Hrubiac, S. Turczynski, D. A. Pawlak, M. Malinowski, D. Wlodarczyk, K. M. Kosyl, W. Paszkowicz, H. Przybylinska, A. Wittlin, A. Kaminska, Y. Zhydashchyy, M. G. Brik, L. Li, C.-G. Ma and A. Suchocki, *Acta Mater.*, 2019, **165**, 346.
- 187 M. J. Weber, *Solid State Commun.*, 1973, **12**, 741.
- 188 J. Ueda, P. Dorenbos, A. J. J. Bos, A. Meijerink and S. Tanabe, *J. Phys. Chem. C*, 2015, **119**, 25003.
- 189 J. Ueda, K. Aishima and S. Tanabe, *Opt. Mater.*, 2013, **35**, 1952.
- 190 T. Horiai, J. Pejchal, J. Paterek, R. Kucerkova, Y. Yokota, A. Yoshikawa and M. Nikl, *Jpn. J. Appl. Phys.*, 2022, **61**, 072002.
- 191 M. Jiao, W. Lv, L. Wei, Q. Zhao, B. Shao and H. You, *Chem. Phys. Chem.*, 2015, **16**, 817.
- 192 I. Venevtsev, V. Khanin, P. Rodnyi, H. Wiczcerek and C. Ronda, *IEEE Trans. Nucl. Sci.*, 2018, **65**, 2090.
- 193 J. M. Ogieglo, *Luminescence and energy transfer in garnet scintillators*, Thesis, University of Utrecht, 2012.
- 194 K. Kamada, T. Endo, K. Tsutumi, T. Yanagida, Y. Fujimoto, A. Fukabori, A. Yoshikawa, J. Pejchal and M. Nikl, *Cryst. Growth Des.*, 2011, **11**, 4484.
- 195 T. Lesniewski, S. Mahlik, K. Asami, J. Ueda, M. Grinberg and S. Tanabe, *Phys. Chem. Chem. Phys.*, 2018, **20**, 18380.
- 196 J. Ueda, P. Dorenbos, A. J. J. Bos, K. Kuroishi and S. Tanabe, *J. Mater. Chem. C*, 2015, **3**, 5642.
- 197 A. Wittlin, H. Przybylinska, M. Berkowski, A. Kaminska, P. Nowakowski, P. Sybilski, C.-G. Ma, M. G. Brik and A. Suchocki, *Opt. Mater. Express*, 2015, **5**, 243542.
- 198 X. Liu, X. Wang and W. Shun, *Phys. Status Solidi A*, 1987, **101**, K161.
- 199 V. Jary, E. Mihokova, M. Nikl, P. Bohacek, A. Lauria and A. Vedda, *Opt. Mater.*, 2010, **33**, 149.
- 200 A. A. Setlur and U. Happek, *J. Solid State Chem.*, 2010, **183**, 1127.
- 201 Y. Chen, K. W. Cheah and M. Gong, *J. Lumin.*, 2011, **131**, 1770.
- 202 Q. Zhang, H. Ni, L. Wang and F. Xiao, *ECS J. Solid State Sci. Technol.*, 2016, **5**, R34.
- 203 H. Luo, A. J. J. Bos and P. Dorenbos, *J. Phys. Chem. C*, 2017, **121**, 8760.
- 204 A. Bessiere, P. Dorenbos, C. W. E. van Eijk, E. Yamagishi, C. Hidaka and T. Takizawa, *J. Electrochem. Soc.*, 2004, **151**, H254.
- 205 B. Dierre, R.-J. Xie, N. Hirosaki and T. Sekiguchi, *J. Mater. Res.*, 2007, **22**, 1933.
- 206 L. Zhang, J. Zhang, X. Zhang, Z. Hao, H. Zhao and Y. Luo, *ACS Appl. Mater. Interfaces*, 2013, **5**, 12839.
- 207 T. Suehiro, N. Hirosaki and R.-J. Xie, *ACS Appl. Mater. Interfaces*, 2011, **3**, 811.
- 208 T. Suehiro, N. Hirosaki, R.-J. Xie and T. Sato, *Appl. Phys. Lett.*, 2009, **95**, 051903.
- 209 J. Ueda and S. Tanabe, *Opt. Mater.: X*, 2019, **1**, 100018.
- 210 P. Dorenbos, *J. Lumin.*, 2000, **91**, 155.
- 211 P. Dorenbos, *J. Lumin.*, 2013, **135**, 93.
- 212 P. Dorenbos, *J. Lumin.*, 2013, **136**, 122.
- 213 P. Dorenbos and E. van der Kolk, *Opt. Mater.*, 2008, **30**, 1052.
- 214 K. Wang, K. P. O'Donnell, B. Hourahine, R. W. Martin, I. M. Watson, K. Lorenz and E. Alves, *Phys. Rev. B: Condens. Matter Mater. Phys.*, 2009, **80**, 125206.
- 215 J. Ueda, A. Meijerink, P. Dorenbos, A. J. J. Bos and S. Tanabe, *Phys. Rev. B*, 2017, **95**, 014303.
- 216 E. van der Kolk, P. Dorenbos, C. W. E. van Eijk, S. A. Basun, G. F. Imbusch and W. M. Yen, *Phys. Rev. B: Condens. Matter Mater. Phys.*, 2005, **71**, 165120.

